



# Hydroelastic design contour for the preliminary design of very large floating structures



Jin-Gyun Kim, Seong-Pil Cho, Ki-Tae Kim, Phill-Seung Lee\*

Division of Ocean Systems Engineering, Korea Advanced Institute of Science and Technology, 291 Daehak-ro, Yuseong-gu, Daejeon 305-701, Republic of Korea

## ARTICLE INFO

### Article history:

Received 29 January 2013

Accepted 2 November 2013

Available online 11 December 2013

### Keywords:

Very large floating structures

Hydroelastic analysis

Preliminary design

Response contour

Design contour

Bending moment

## ABSTRACT

In this paper, we propose a hydroelastic design contour (HDC) that can be practically used for the preliminary design of pontoon-type rectangular very large floating structures (VLFSS). Using the design contour, we can easily predict the maximum bending moment of VLFSS in irregular waves. To develop the design contour, we first construct the hydroelastic response contours (HRCs) by extensively carrying out hydroelastic analyses considering various structural and wave conditions, namely, the bending stiffness and aspect ratio of VLFSS, incident wave length and angle, as well as the sea state. Based on the pre-calculated HRCs, we develop the HDC considering irregular waves. We then propose a preliminary design procedure for VLFSS using the HDC and demonstrate the design procedure for pontoon-type rectangular VLFSS. The HDC can significantly reduce time and effort for the design of VLFSS.

© 2013 Elsevier Ltd. All rights reserved.

## 1. Introduction

Very large floating structures (VLFSS) have attracted many engineers since the concept appeared in the 19th century. VLFSS can be used as platforms for various offshore facilities such as oil storages, container terminals and airports. Cost effectiveness, movability, and environmental-friendly features could be the representative advantages of VLFSS compared with land reclamation. Recently, several challenging projects to develop VLFSS have been carried out such as Mobile Offshore Base (ONR, 1997~2000), Mega-Float (TRAM, 1995~2001), Modular Hybrid Pier (NFESC, 1998~2004), and Hybrid Quay Wall (KIOST, 2005–2009). However, the design procedures and regulations for the construction of VLFSS have not been well established yet.

In the design of VLFSS, hydroelastic analysis is required to evaluate the responses of the floating structures in waves because VLFSS have relatively small bending rigidity compared to the overall dimensions of the structures. Therefore, the complicated interaction between water waves and flexible structures should be appropriately considered to calculate the structural responses of VLFSS.

The fundamental theory of hydroelastic analysis was established for ship design in the 1980s (Bishop and Price, 1979). The methods of hydroelastic analysis for VLFSS have been actively studied as reviewed in ISSC (2006) and Watanabe et al. (2004). In most studies on hydroelastic analysis, VLFSS have been assumed to be relatively simple floating beam and plate structures

(Kashiwagi, 1998; Khabakhpasheva and Korobkin, 2002; Kim et al., 2007; Eatock Taylor, 2007). Recently, VLFSS have been modeled as three-dimensional floating structures (Riggs et al., 2007; Kim et al., 2013). In general, fluid has been modeled by the potential fluid theory.

In hydroelastic analysis, fluid and structures should be handled together. Therefore, additional modeling effort and computational time are required. In the cross-section design of VLFSS, the maximum bending moment that occurs in VLFSS in the ranges of wave parameters should be calculated through hydroelastic analysis and compared with the bending moment capacity of the cross-section. Until the safety requirement is properly satisfied, hydroelastic analyses have to be iteratively performed under various structural and wave conditions.

For a typical design example, when the ranges of the incident wave length and angle are divided into 50 and 51 cases, respectively, 2550 cases of the hydroelastic analysis should be performed. To construct the wave spectrums for various irregular wave conditions, additional computational cost is required. Assuming that 4 design trials are necessary to satisfy the safety requirement, in total 10,200 ( $4 \times 2550$ ) cases of hydroelastic analysis should be carried out (Kim et al., 2011). Of course, it is also a difficult task for engineers to process all the data obtained in the analyses for the design purpose. This fact motivates this study.

The objective of this paper is to propose a very useful design tool, hydroelastic design contour (HDC), that can significantly reduce engineers' effort and time for the preliminary design of pontoon-type rectangular VLFSS.

In this study, VLFSS are simplified as two-dimensional floating isotropic plates instead of more realistic orthotropic plates or full

\* Corresponding author. Tel.: +82 42 350 1512; fax: +82 42 350 1510.  
E-mail address: [phillseung@kaist.edu](mailto:phillseung@kaist.edu) (P.-S. Lee).

three dimensional shell structures. The water depth is assumed to be infinite. We construct two types of hydroelastic response contours (HRC-I and HRC-II) to estimate the response amplitude operator (RAO) of the maximum bending moment for a given geometry and bending stiffness of VLFS. HRC-I shows the RAO of the maximum bending moment depending on wave length and angle. However, HRC-II shows the RAO of the maximum bending moment under given ranges of wave length and angle. Based on HRCs, we then construct HDC to estimate the maximum bending moment in irregular waves. The Beaufort scale and the corresponding JONSWAP wave spectrum are used to consider irregular wave effects in HDC.

The bending moments predicted by HDC can be used for the preliminary design of VLFSs. We also establish a new design procedure based on the HDC. The new design procedure can significantly reduce modeling effort and computational time in the design of VLFSs because time-consuming hydroelastic analyses do not need to be performed. We verify the design procedure and HDC by performing the preliminary designs of pontoon-type rectangular VLFSs with single and double hulls. We also test the feasibility of the HDC for finite water depth cases through numerical examples.

In the following sections, we first review the governing equations and the numerical procedure that we adopt to solve the hydroelastic problems of floating plate structures. The procedure to develop the hydroelastic response and design contours is explained in detail. We then propose a design procedure using the HDC and the preliminary designs of pontoon-type VLFSs are demonstrated. Finally, the concluding remarks are given.

## 2. Theoretical background

In this section, we briefly present mathematical formulations and discrete coupled equations for the hydroelastic analysis of floating plates interacting with surface regular waves. In this work, the structural motions and the amplitudes of incident waves are assumed to be small enough for the use of linear theory.

Fig. 1 shows the problem description. A plate ( $L \times B \times H$ ) is floating on the water with draft  $d$ . The water depth  $h$  is measured from the flat bottom seabed to the free surface of calm water, and a fixed Cartesian coordinate system ( $x_1, x_2, x_3$ ) on the free surface is introduced. The plate volume is denoted by  $V$ , and the fluid is bounded by the wet surface of the structure  $S_B$ , the free surface  $S_F$ , the surface  $S_\infty$  which is a circular cylinder with a sufficiently large radius  $R$ , and the flat bottom seabed surface  $S_G$ . An incident gravity wave with small amplitude  $a$  and angular frequency  $\omega$  comes continuously from the positive  $x_1$  axis with an angle  $\theta$ . The basic assumptions are that the plate has homogeneous, isotropic, and linear elastic material, and the fluid flow is incompressible, inviscid, and irrotational. In addition, for simplicity, we set the atmospheric pressure to be zero.

### 2.1. Formulation of the floating plate

The equilibrium equations of the floating plate at time  $t$  are

$$\begin{aligned} \frac{\partial^t \sigma_{ij}}{\partial^t x_j} - {}^t \rho_s g \delta_{i3} - {}^t \rho_s {}^t \ddot{u}_i &= 0 & \text{in } {}^t V \\ {}^t \sigma_{ij} n_j &= -{}^t p {}^t n_i & \text{on } {}^t S_B \end{aligned} \quad (1)$$

where  ${}^t \sigma_{ij}$  is the Cauchy stress tensor at time  $t$ ,  ${}^t \rho_s$  is the structural density at time  $t$ ,  $\rho_w$  is the fluid density,  $g$  is the acceleration of gravity,  ${}^t u_i$  is the displacement at time  $t$ , and  ${}^t p$  denotes the total water pressure at time  $t$ . Note that  ${}^t p = -\rho_w g x_3 + {}^t p_d$ , in which  ${}^t p_d$  is the hydrodynamic pressure. Also,  $\delta_{ij}$  is the Kronecker delta, and  ${}^t n_i$  denotes the unit normal vector outward from the plate to the fluid at time  $t$ . We use subscripts  $i$  and  $j$ , which vary from 1 to 3 to

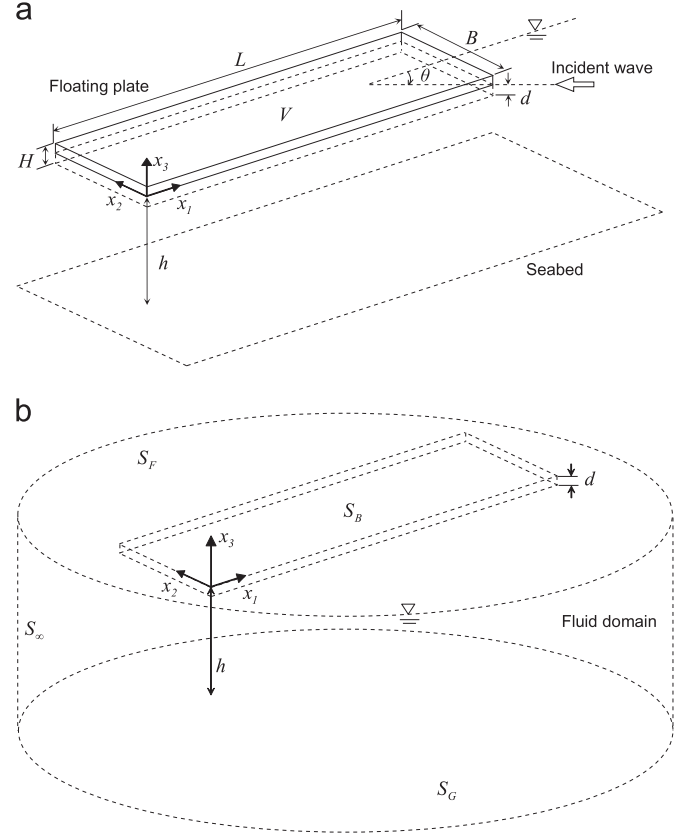


Fig. 1. Problem description for the hydroelastic analysis of a floating plate: (a) floating plate and incident wave and (b) fluid domain with an interface fluid boundary surface.

express the components of tensor, and adopt the Einstein summation convention.

The principle of virtual work for the floating plate at time  $t$  can be stated as

$$\begin{aligned} \int_{{}^t V} {}^t \rho_s^t \ddot{u}_i \delta u_i dV + \int_{{}^t V} {}^t \sigma_{ij} \delta e_{ij} dV \\ = - \int_{{}^t V} {}^t \rho_s g \delta u_3 dV + \int_{{}^t S_B} \rho_w g {}^t x_3 {}^t n_i \delta u_i dS - \int_{{}^t S_B} {}^t p_d {}^t n_i \delta u_i dS, \end{aligned} \quad (2)$$

where  $\delta u_i$  and  $\delta e_{ij}$  refer to the virtual displacement vector and small strain tensor, respectively.

In the hydrostatic equilibrium state, which is denoted by time  $t=0$ , Eq. (2) becomes

$$\int_{{}^0 V} {}^0 \sigma_{ij} \delta e_{ij} dV = - \int_{{}^0 V} {}^0 \rho_s g \delta u_3 dV + \int_{{}^0 S_B} \rho_w g {}^0 x_3 {}^0 n_i \delta u_i dS. \quad (3)$$

If we linearize Eq. (2) at the static equilibrium state, and subtract Eq. (3) from the linearized Eq. (2), we obtain the steady state equation (Kim et al., 2013)

$$\begin{aligned} -\omega^2 \int_{{}^0 V} {}^0 \rho_s u_i \delta u_i dV + \int_{{}^0 V} C_{ijkl} e_{kl} \delta e_{ij} dV - \int_{{}^0 S_B} \rho_w g u_3 {}^0 n_i \delta u_i dS \\ = - \int_{{}^0 S_B} p_d {}^0 n_i \delta u_i dS, \end{aligned} \quad (4)$$

where  $C_{ijkl}$  is the stress-strain relation tensor ( $k$  and  $l$  vary from 1 to 3), and

$${}^t u_i = {}^t x_i - {}^0 x_i = \text{Re}\{u_i e^{j\omega t}\}, \quad {}^t e_{ij} = \text{Re}\{e_{ij} e^{j\omega t}\}, \quad {}^t p_d = \text{Re}\{p_d e^{j\omega t}\} \quad (5)$$

in which the superscript  $j = \sqrt{-1}$ . Note that in Eq. (4), we assume that  ${}^0x_3$  and  ${}^0\sigma_{ij}$  are equal to zero because they are negligible quantities.

## 2.2. Formulation of the fluid

In the steady state, the velocity potential  ${}^t\phi$  is governed by

$${}^t\phi = \text{Re}\{\phi e^{j\omega t}\} \quad (6a)$$

$$\nabla\phi^2 = 0 \quad \text{in fluid domain,} \quad (6b)$$

$$\frac{\partial\phi}{\partial x_3} = \frac{\omega^2}{g}\phi \quad \text{for } x_3 = 0 \text{ on } S_F, \quad (6c)$$

$$\frac{\partial\phi}{\partial x_3} = 0 \quad \text{on } S_G, \quad (6d)$$

$$\sqrt{R}\left(\frac{\partial}{\partial R} + jk\right)(\phi - \phi_1) = 0 \quad \text{on } S_\infty \quad (R \rightarrow \infty), \quad (6e)$$

$$\frac{\partial\phi}{\partial n} = -j\omega u_3 \quad \text{on } {}^0S_B \quad (6f)$$

where  $\nabla$  is the Laplace operator,  $k$  is the wave number and  $\phi_1$  is the velocity potential for the incident wave. The incident velocity potential  $\phi_1$  is defined by (Dean and Dalrymple, 1984; Wehausen and Laitone, 1960)

$$\phi_1 = j\frac{ga}{\omega} \frac{\cosh k(x_3 + h)}{\cosh kh} e^{jk(x_1 \cos \theta + x_2 \sin \theta)} \quad (7)$$

From Eqs. (6) and (7), the boundary integral equation can be formulated using Green's function and Green's second identity (Kim et al., 2013). The boundary integral equation for the floating plate is

$$4\pi\phi - 4\pi\phi_1 = \int_{{}^0S_B} \left( -\phi \frac{\omega^2}{g} G - G \frac{\partial\phi}{\partial n} \right) dS_\xi \quad (8)$$

where  $G(\mathbf{x}, \xi)$  is the free surface Green's function (Wehausen and Laitone, 1960), and this is a function of spatial point  $\mathbf{x}$  and source point  $\xi$ . The subscript  $\xi$  means that the integral should be conducted with respect to  $\xi$ .

Using the linearized Bernoulli equation, the velocity potential  $\phi$  is expressed as

$$\phi = j\left(\frac{1}{\rho_w} p + g u_3\right) \quad \text{on } {}^0S_B, \quad (9)$$

where  ${}^t p = \text{Re}\{p e^{j\omega t}\}$ . If we insert Eqs. (9) and (6f) into Eq. (8), we have

$$\frac{p}{\rho_w g} + u_3 + \frac{\omega^2}{4\pi\rho_w g^2} \int_{{}^0S_B} p G dS_\xi = -j\frac{\omega}{g} \phi_1 \quad \text{on } {}^0S_B, \quad (10)$$

For subsequent boundary element approximations, we weight a test function  $\delta p$  to Eq. (10), and integrate over the wet surface  ${}^0S_B$

$$\begin{aligned} & \frac{1}{\rho_w g} \int_{{}^0S_B} p \delta p dS + \int_{{}^0S_B} u_3 \delta p dS + \frac{\omega^2}{4\pi\rho_w g^2} \int_{{}^0S_B} \int_{{}^0S_B} p G dS_\xi \delta p dS_x \\ & = -j\frac{\omega}{g} \int_{{}^0S_B} \phi_1 \delta p dS. \end{aligned} \quad (11)$$

## 2.3. Discretization of the coupled equations

The formulations in Eqs. (4) and (11) can be transformed into the coupled matrix form by the finite and boundary element discretizations as

$$\begin{bmatrix} -\omega^2 \mathbf{S}_M + \mathbf{S}_K & -\mathbf{C}_{up} \\ -\mathbf{C}_{up}^T & -\mathbf{F}_M - \mathbf{F}_G \end{bmatrix} \begin{bmatrix} \hat{\mathbf{u}} \\ \hat{\mathbf{p}} \end{bmatrix} = \begin{bmatrix} \mathbf{0} \\ \hat{\mathbf{R}}_I \end{bmatrix} \quad (12)$$

in which the matrices and vectors are defined as follows:

$$\omega^2 \int_{{}^0V} {}^0\rho_s u_i \delta u_i dV = \delta \hat{\mathbf{u}}^T \omega^2 \mathbf{S}_M \hat{\mathbf{u}} \quad (13a)$$

$$\int_{{}^0V} C_{ijkl} e_{kl} \delta e_{ij} dV = \delta \hat{\mathbf{u}}^T \mathbf{S}_K \hat{\mathbf{u}} \quad (13b)$$

$$\int_{{}^0S_B} p \delta u_3 dS = \delta \hat{\mathbf{u}}^T \mathbf{C}_{up} \hat{\mathbf{p}} \quad (13c)$$

$$\frac{1}{\rho_w g} \int_{{}^0S_B} p \delta p dS = \delta \hat{\mathbf{p}}^T \mathbf{F}_M \hat{\mathbf{p}}, \quad (13d)$$

$$\frac{\omega^2}{4\pi\rho_w g^2} \int_{{}^0S_B} \int_{{}^0S_B} p G dS_\xi \delta p dS_x = \delta \hat{\mathbf{p}}^T \mathbf{F}_G \hat{\mathbf{p}} \quad (13e)$$

$$j\frac{\omega}{g} \int_{{}^0S_B} \phi_1 \delta p dS = \delta \hat{\mathbf{p}}^T \hat{\mathbf{R}}_I \quad (13f)$$

Note that, in the discretization for the steady state problem, the structural finite element and the fluid boundary element should be matched each other on the wet surface  ${}^0S_B$ . To discretize the coupled equations, we here use the 4-node MITC shell finite element (MITC4), in which the MITC (Mixed Interpolation of Tensorial Components) method is applied to alleviate undesired shear locking phenomena (Bathe and Dvorkin, 1986; Bathe, 1996; Bathe and Lee, 2001; Bathe et al., 2003; Lee and Bathe, 2004, 2010; Lee et al., 2007, 2012).

In Kim et al. (2013), the formulation reviewed in this section were verified through comparisons with the experimental results obtained by Yago and Endo (1996).

## 3. Hydroelastic response contours

The hydroelastic design contour (HDC) is constructed based on the hydroelastic response contours (HRCs). In this section, we propose two types of HRC (HRC-I and HRC-II).

### 3.1. Hydroelastic response contour – I

Here, we describe how to develop the HRC-I, which can give the RAO of the dimensionless maximum bending moment depending on incident regular wave length and angle for the given structural parameters.

VLFSSs are assumed to be two-dimensional rectangular floating plates of length  $L$ , breadth  $B$ , and height  $H$ . The water depth  $h$  is assumed to be infinite.

At a certain position  $(x_1, x_2)$  in the plate, the maximum principal bending moment per unit width is defined by

$$\begin{aligned} M_p(x_1, x_2) &= \max(|M_1(x_1, x_2)|, |M_2(x_1, x_2)|) \quad \text{with} \\ M_{1,2} &= \frac{M_{x_1} + M_{x_2}}{2} \pm \sqrt{\left(\frac{M_{x_1} - M_{x_2}}{2}\right)^2 + M_{x_1 x_2}^2} \end{aligned} \quad (14)$$

where  $M_{x_1}$  and  $M_{x_2}$  are the bending moments,  $M_{x_1 x_2}$  is the twisting moment, and  $M_1$  and  $M_2$  are the principal bending moments (Timoshenko and Krieger, 1970). Note that all the bending moments considered in this study are per unit width.

Let us consider the maximum bending moment  $M_{\text{max}}$ , which is the maximum value in the distribution of the maximum principal bending moment  $M_p$  in the entire plate domain ( $0 \leq x_1 \leq L$  and  $0 \leq x_2 \leq B$ ) under incident wave with unit amplitude ( $a=1$ ). That is,  $M_{\text{max}}$  is the RAO of the maximum bending moment. Then, the RAO of the dimensionless maximum bending moment denoted as

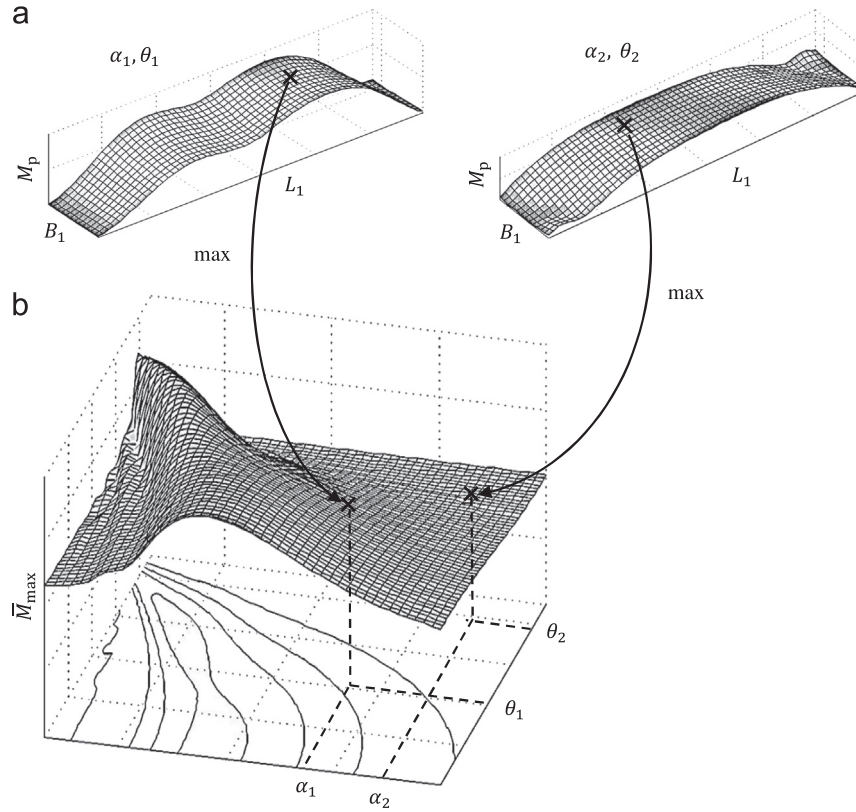


**Fig. 2.** Construction procedure of the HRC-I for the case of  $L_1/B_1$  and  $S_1$ . (a) distribution of the maximum principal bending moment in the floating plate under two wave cases and (b) HRC-I.

$\bar{M}_{\max}$  is a function of 5 dimensionless parameters

$$\bar{M}_{\max} = \bar{M}_{\max}(L/B, S, d/H, \alpha, \theta) \quad \text{with} \quad \bar{M}_{\max} = \frac{M_{\max}}{\rho_w g L^2} \quad (15)$$

where  $L/B$  is the aspect ratio,  $S = EI/\rho_w g L^5$  is the dimensionless bending stiffness<sup>1</sup> with Young's modulus  $E$  and the second moment of inertia  $I$  ( $I = BH^3/12$ ),  $d/H$  is the ratio of draft to height,  $\alpha = \lambda/L$  is the ratio of wave length to structural length, and  $\theta$  is the angle of the incident wave (Lee and Newman, 2000).

In Eq. (15), the ratio  $d/H$  represents the ratio of plate density to fluid density. Considering the practical range of  $d/H$ , we assume  $d/H = 0.5$ , which means that draft  $d$  is half of the plate height. Then, for the given  $d/H$ , Eq. (15) becomes

$$\bar{M}_{\max} = \bar{M}_{\max}(L/B, S, \alpha, \theta) \quad (16)$$

Based on Eq. (16), HRC-I is designed to present the RAO of the dimensionless maximum bending moment for the given  $L/B$  and  $S$  depending on  $\alpha$  and  $\theta$ .

For the given  $S$  and  $L/B$ , Fig. 2 shows how to construct HRC-I. Changing the values  $\alpha$  and  $\theta$ , we find the maximum values in the RAO distribution of the maximum principal bending moment  $M_p$  and plot them in HRC-I as shown in Fig. 2(a) and (b). Therefore, HRC-I presents the RAO of the dimensionless maximum bending moment as a function of  $\alpha$  and  $\theta$  for the given structural parameters.

Figs. 3 and 4 display HRC-I considering four aspect ratios  $L/B = 1, 2.5, 5$  and  $7.5$ , and three dimensionless stiffness parameters

$S = 2 \times 10^{-5}, 1 \times 10^{-4}$  and  $2 \times 10^{-4}$ . To calculate all the hydroelastic responses, the floating plates are modeled by the plate finite elements with  $60 \times 60$  mesh for  $L/B = 1$ ,  $60 \times 24$  mesh for  $L/B = 2.5$ ,  $60 \times 12$  mesh for  $L/B = 5$ , and  $60 \times 8$  mesh for  $L/B = 7.5$ . In order to obtain the proper meshes, the convergence of the maximum bending moments was tested for the smallest wave length cases considered ( $\alpha = 0.04$ ). The meshes chosen can provide less than 3% errors in the maximum bending moments compared to well-converged solutions. Note that much finer meshes would be required to accurately calculate entire bending moment distributions in the floating plates (Wang et al., 2008).

HRC-I can also give the values of  $\alpha$  and  $\theta$  when the maximum bending moment occurs. Many valuable detailed investigations can be made through HRC-I. Here we particularly note an important observation that the maximum bending moment occurs when the dimensionless wave length  $\alpha$  varies from 0.04 to 1.0 in the analysis cases considered. The contours also show that, as the bending stiffness increases, the wave length corresponding to the maximum bending moments becomes closer to  $L$ . HRC-I shows how the bending moment distribution varies according to  $S$  and  $L/B$  in detail.

### 3.2. Hydroelastic response contour - II

Based on the HRC-I, HRC-II is constructed to estimate the RAO of the dimensionless maximum bending moment in the significant ranges of wave length  $\alpha$  and angle  $\theta$ . When the ranges of  $\alpha$  and  $\theta$  in Eq. (16) are fixed, the RAO of the dimensionless maximum bending moment becomes only a function of  $L/B$  and  $S$

$$\bar{M}_{\max} = \bar{M}_{\max}(L/B, S) \quad (17)$$

The ranges of the wave parameters should be carefully determined to properly consider the hydrodynamic effects on VLFs in the

<sup>1</sup> Note that the bending stiffness of isotropic plates is defined by  $D = EH^3/12(1 - \nu^2)$  per unit width in general. However, in this study we use the longitudinal bending stiffness  $EI$  as a representative bending stiffness by fixing Poisson's ratio  $\nu = 0.3$ .

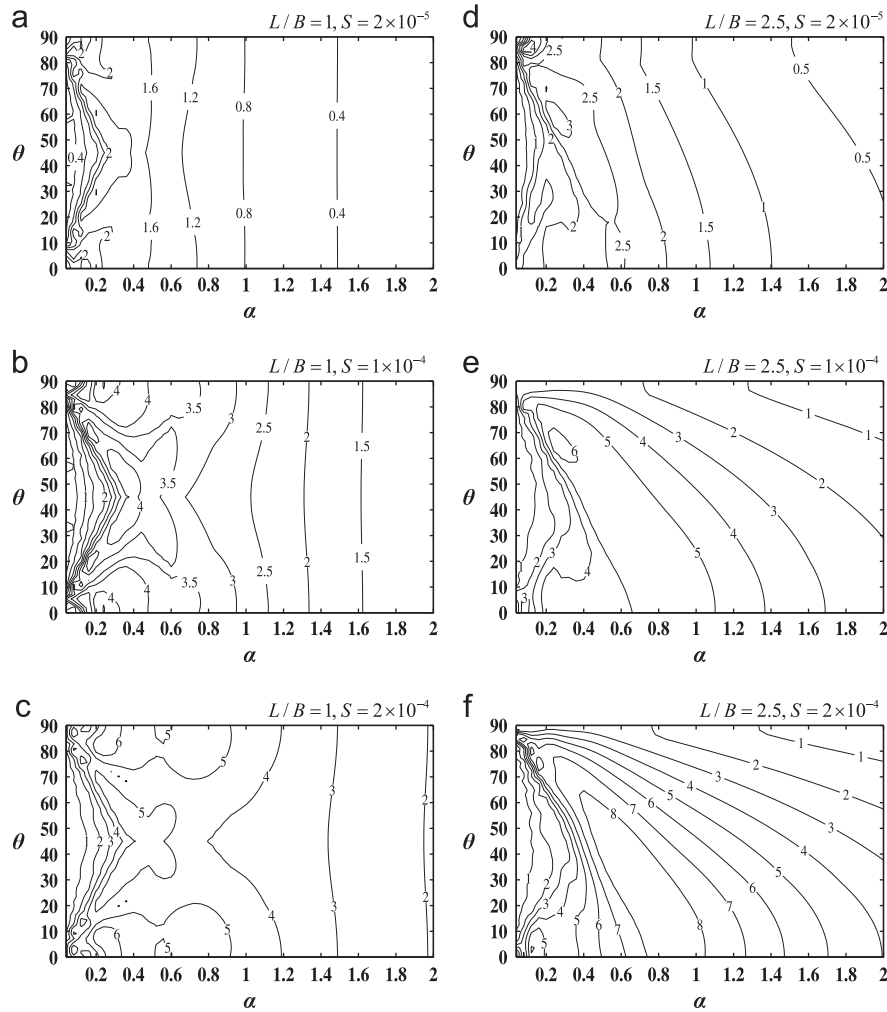


Fig. 3. HRC-I for  $\bar{M}_{\max}$  ( $\times 10^{-3}$ ). (a)  $L/B=1$  and  $S=2 \times 10^{-5}$ , (b)  $L/B=1$  and  $S=1 \times 10^{-4}$ , (c)  $L/B=1$  and  $S=2 \times 10^{-4}$ , (d)  $L/B=2.5$  and  $S=2 \times 10^{-5}$ , (e)  $L/B=2.5$  and  $S=1 \times 10^{-4}$  and (f)  $L/B=2.5$  and  $S=2 \times 10^{-4}$ .

preliminary design stage. In this study, the range of the wave angle  $\theta$  that we choose is from  $0^\circ$  to  $90^\circ$  because the shape of the VLFSS considered is symmetric. We use the range of the dimensionless wave length  $\alpha$  from 0 to 2. This is a reasonable choice for most of VLFSS because, in general, the bending moment is maximum when  $0 < \alpha < 1$  as investigated in the previous section. Table 1 also shows that the wave parameters in previous studies on VLFSS design are mostly covered by those ranges (Yago and Endo, 1996; Hong, 2007).

Fig. 5 shows how HRC-II is developed from HRC-I. For the given range of wave parameters ( $0 \leq \theta \leq 90^\circ$  and  $0 < \alpha \leq 2$ ), HRC-I is prepared by changing the values of  $L/B$  and  $S$  as shown in Fig. 5(a). Then, the maximum RAO of the dimensionless maximum bending moment is found in each HRC-I and plotted in HRC-II as shown in Fig. 5(b). The horizontal and vertical axes of HRC-II are the dimensionless bending stiffness  $S$  and the aspect ratio  $L/B$  of VLFSS, respectively. Hence, HRC-II can give the RAO of the dimensionless maximum bending moment with respect to the structural parameters,  $L/B$  and  $S$ , for the given ranges of the wave parameters.

Considering the aspect ratio  $1 \leq L/B \leq 10$  and the dimensionless bending stiffness  $2 \times 10^{-6} \leq S \leq 2 \times 10^{-4}$ , Fig. 6 presents the HRC-II. To plot HRC-II, we performed hydroelastic analyses considering 7 aspect ratios ( $L/B=1, 2.5, 4, 5, 6, 7.5$  and  $10$ ) and 7 dimensionless stiffness parameters ( $S=2 \times 10^{-6}, 1 \times 10^{-5}, 2 \times 10^{-5}, 5 \times 10^{-5}, 1 \times 10^{-4}, 1.5 \times 10^{-4}$  and  $2 \times 10^{-4}$ ). The ranges of the incident wave length and angle are divided into 50 and 51 cases with a

uniform interval, respectively. Therefore,  $\alpha=0.04, 0.08, 0.12, \dots, 2.0$  (from 0.04 to 2) and  $\theta=0, 1.8, 3.6, \dots, 90^\circ$ . To construct HRC-II, a total of 124,950 ( $7 \times 7 \times 51 \times 50$ ) cases of hydroelastic analysis were performed. Table 1 shows that the structural parameters in the previous studies are sufficiently contained in the ranges considered in this study.

#### 4. Hydroelastic design contour and design procedure

In this section, we propose the hydroelastic design contour (HDC), which is constructed based on the HRCs discussed in the previous section. HDC is developed to estimate the maximum bending moments of VLFSS in irregular waves. We also propose a preliminary design procedure using HDC.

##### 4.1. Hydroelastic design contour

Real water waves in the ocean are irregular. Therefore, the effect of the irregular waves should be considered in the design of VLFSS. HDC is constructed from HRCs to estimate the maximum bending moment in irregular waves represented by sea states.

The irregular waves can be statistically represented by wave spectrums. We adopt the Mean JONSWAP wave spectrum (Journée

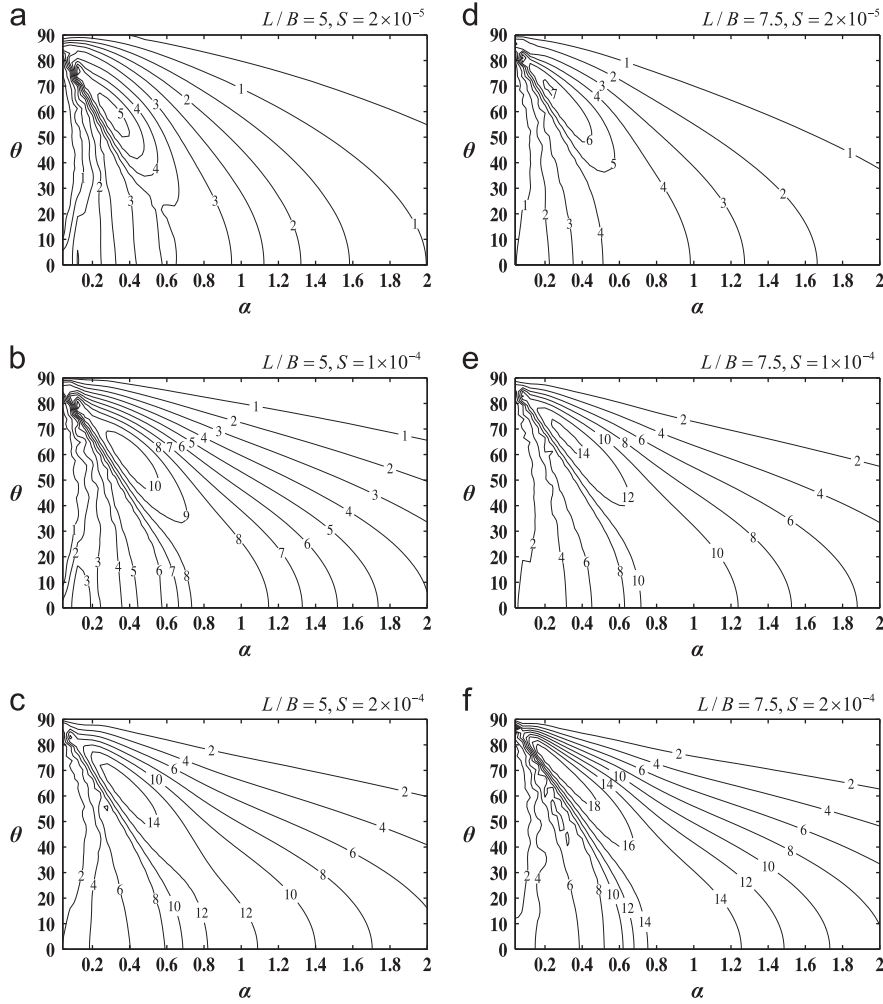


**Fig. 4.** HRC-I for  $\bar{M}_{\max}$  ( $\times 10^{-3}$ ). (a)  $L/B = 5$  and  $S = 2 \times 10^{-5}$ , (b)  $L/B = 5$  and  $S = 1 \times 10^{-4}$ , (c)  $L/B = 5$  and  $S = 2 \times 10^{-4}$ , (d)  $L/B = 7.5$  and  $S = 2 \times 10^{-5}$ , (e)  $L/B = 7.5$  and  $S = 1 \times 10^{-4}$  and (f)  $L/B = 7.5$  and  $S = 2 \times 10^{-4}$ .

**Table 1**  
Ranges of the design parameters in previous researches on VLFS designs.

	$h$ (m)	$d/H$	$L/B$	$S$	$\alpha$	$\theta$ (deg)
Mega-Float (Yago and Endo, 1996)	58.5	0.25	5.0	$1.96 \times 10^{-5}$	0.1~1.0	0, 30, 60, 90
KIOST (Hong, 2007)	8	0.5	1.7	$5.0 \times 10^{-5}$	0.09~0.44	0~90
	30	0.33	2.0	$7.0 \times 10^{-6}$	0.13~0.34	0~90

and Massie, 2001)

$$S_j(\omega) = \frac{320 (H_{1/3})^2}{T_p^4} \omega^{-5} \exp\left(-\frac{1950}{T_p^4} \omega^{-4}\right) \gamma^4 \quad \text{with}$$

$$A = \exp\left\{-\left(\frac{\omega/\omega_p - 1}{\sigma\sqrt{2}}\right)^2\right\}, \omega_p = \frac{2\pi}{T_p} \quad \text{and} \quad \sigma = \begin{cases} 0.07 & \text{if } \omega \leq \omega_p \\ 0.09 & \text{if } \omega > \omega_p \end{cases} \quad (18)$$

where  $H_{1/3}$  is the significant wave height,  $\gamma$  is the peakedness factor ( $\gamma=3.3$ ).  $\omega_p$  and  $T_p$  are the peak frequency and period at the spectral peak, respectively. Note that  $T_p$  can be calculated from the mean centroid wave period  $T_1$ . The relation between  $T_p$  and  $T_1$  is

$$T_1 = 0.834T_p \quad (19)$$

Table 2 shows the relation between the sea states defined by the Beaufort scale and the characteristic data of the JONSWAP wave spectrum (Journée and Massie, 2001). The Beaufort scale is an

empirical measure that relates the average wind velocity at 19.5 m above the sea level to observed sea conditions.

The JONSWAP wave spectrum  $S_j^{(k)}$  at sea state  $k$  can be calculated by Eqs. (18) and (19), and the characteristic data in Table 2. The wave energy spectrum at sea state  $k$  is defined as

$$S_j^{(k)}(\omega) d\omega = \frac{1}{2} (a^{(k)}(\omega))^2 \quad (20)$$

Similarly, the energy spectrum of the dimensionless bending moment can be defined

$$S_M^{(k)}(\omega) = (\bar{M}_{\max}(\omega))^2 S_j^{(k)}(\omega) \quad (21)$$

where  $S_M^{(k)}$  is the energy spectrum of the dimensionless bending moment at sea state  $k$ , and  $\bar{M}_{\max}$  is the RAO of the dimensionless maximum bending moment in HRC-II. That is,  $\bar{M}_{\max}$  is a transfer

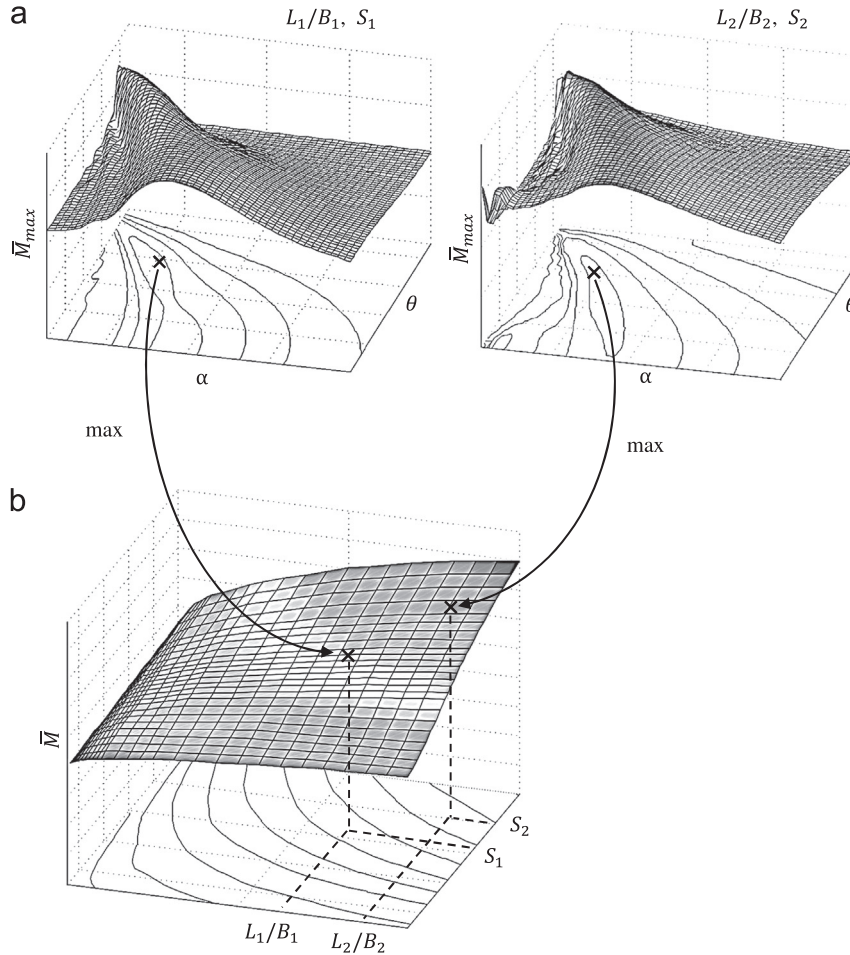


Fig. 5. Construction procedure of the HRC-II. (a) HRC-I for two cases of  $L/B$  and  $S$  and (b) HRC-II.

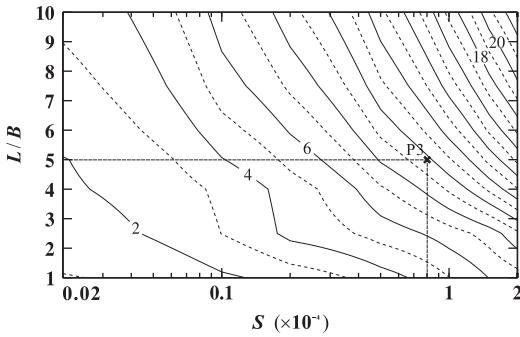


Fig. 6. HRC-II for  $\bar{M}_{\max}$  ( $\times 10^{-3}$ ). P3 denotes the third trial to estimate  $\bar{M}_{\max}$ , see Section 5 and Table 4.

function to give the relation between bending moment and wave spectrum.

The dimensionless maximum bending moment at sea state  $k$  is finally calculated using Eq. (21), and the mean response height of the one third highest responses

$$\bar{M}_{\max}^{(k)} = \frac{2}{a_{1/3}^{(k)}} \left[ \int_0^\infty S_M^{(k)}(\omega) d\omega \right]^2 \quad (22)$$

in which  $a_{1/3}^{(k)}$  is the significant wave amplitude ( $a_{1/3}^{(k)} = H_{1/3}^{(k)}/2$ ) at sea state  $k$ .

In this paper, we construct HDC corresponding to sea states 5–10. Sea state 10 can be regarded as the most severe sea condition for VLFSS, and this means storm condition in the US weather service description.

Table 2  
Relation between the Beaufort wind scale and the characteristic data of the JONSWAP wave spectrum (Journée and Massie, 2001).

Sea state number	Wind speed (kn)	Significant wave height $H_{1/3}$ (m)	Mean centroid wave period $T_1$ (s)
1	2.0	0.50	3.50
2	5.0	0.65	3.80
3	8.5	0.80	4.20
4	13.5	1.10	4.60
5	19.0	1.65	5.10
6	24.5	2.50	5.70
7	30.5	3.60	6.70
8	37.0	4.85	7.90
9	44.0	6.10	8.80
10	51.5	7.45	9.50
11	59.5	8.70	10.00
12	> 64.0	10.25	10.50

The ranges of the structural and wave parameters used for HDC are identical to those of HRC-II. Therefore, considering the range  $0.04 \leq \alpha \leq 2$  in the JONSWAP wave spectrum, the zero order moment  $m_0^{(k)}$  is calculated as

$$m_0^{(k)} = \int_{\omega_1}^{\omega_2} S_j^{(k)} d\omega \quad (23)$$

in which  $\omega_1$  and  $\omega_2$  are the wave frequencies corresponding to  $\alpha=0.04$  and  $\alpha=2$ . The calculated zero order moments are above 99% of the analytical values  $\int_0^\infty S_j^{(k)} d\omega$  in sea states 5–10. This means that the spectrum energy is well reflected in the range of  $\alpha$ .

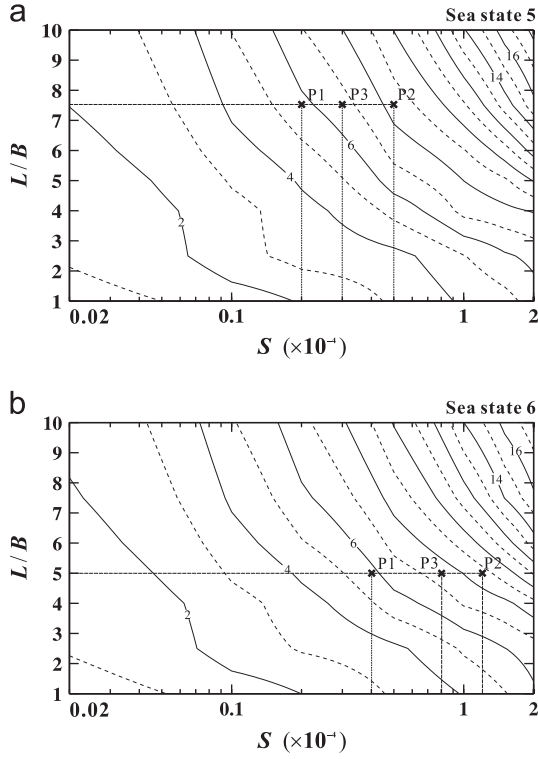


Fig. 7. HDC for  $\bar{M}_{\max}^{(k)}$  ( $\times 10^{-3}$ ). (a) Sea state 5, (b) Sea state 6. P1, P2, and P3 denote the first, second, and third trials in the two design demonstrations, see Section 5 and Tables 3–5.

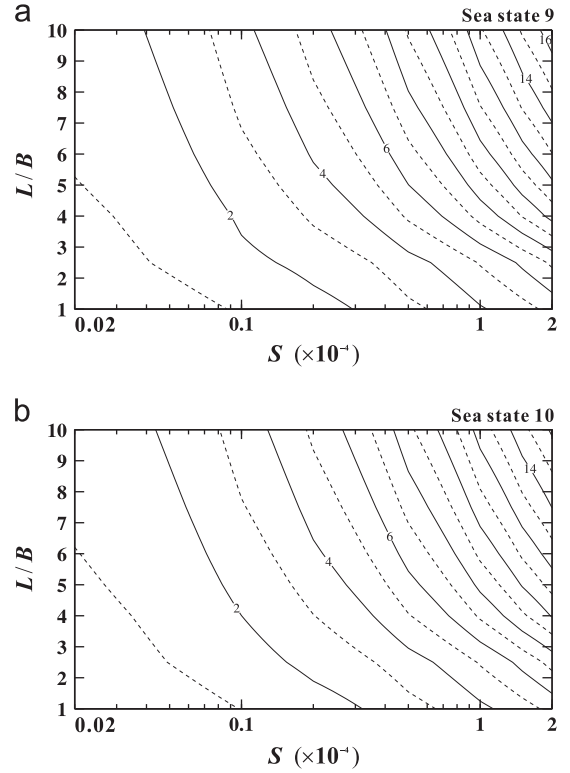


Fig. 9. HDC for  $\bar{M}_{\max}^{(k)}$  ( $\times 10^{-3}$ ). (a) Sea state 9 and (b) Sea state 10.

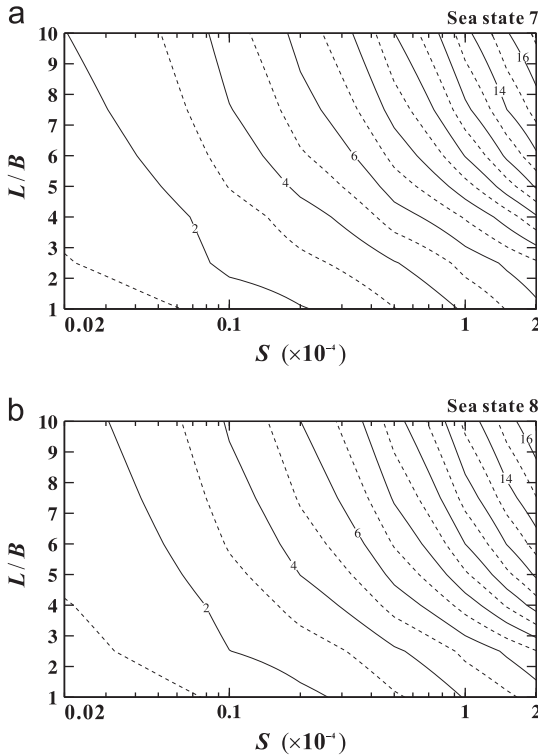


Fig. 8. HDC for  $\bar{M}_{\max}^{(k)}$  ( $\times 10^{-3}$ ). (a) Sea state 7 and (b) Sea state 8.

The horizontal and vertical axes of HDC correspond to the dimensionless bending stiffness  $S$  and aspect ratio  $L/B$ , respectively. Using the procedure in Eq. (22), the dimensionless maximum bending moment in each sea state is calculated and plotted

in HDC. Figs. 7–9 show the proposed HDC corresponding to sea states 5–10, which can give the dimensionless maximum bending moment of VLFSs in each sea state without numerical analysis in the preliminary design stage.

Based on HRC-II, HDC can be constructed by other wave spectra such as ISSC, SMB and TMA models considering adequate environmental conditions for the operation of VLFSs. Using a procedure similar to that presented in this paper, the HRCs and HDC for other structural responses such as maximum stress, displacement, and acceleration can be constructed for the purposes of design and detailed investigation of the hydroelastic response of VLFSs.

#### 4.2. New design procedure

In this section, we propose a new hydroelastic design procedure using HDC as shown in Fig. 10. Note that the use of the design procedure is restricted in the preliminary design stage.

In the design procedure, step 1 is for the initial plan of a VLFS. Overall dimensions, such as structural length  $L$  and width  $B$ , are determined for the service purpose of VLFS. To estimate the maximum bending moment at a significant sea state by using HDC, the significant sea state is also determined according to the sea area in which the VLFS operates.

In step 2, an initial structural design for the cross-section is performed. The compartments and members are arranged, and the dimensions of decks and stiffeners are determined in this step. The materials of all members are also defined. Then, the dimensionless bending stiffness  $S$  and bending moment capacity  $M_u$  are calculated.

In step 4, the maximum bending moments  $M_{\max}$  due to the wave conditions at the sea state are estimated using HDC.

In step 5, the structural safety of the VLFS is checked considering the bending moment capacity  $M_u$  and the maximum bending moment  $M_{\max}$ . Unless  $M_u$  is large enough to satisfy the required safety criteria, the design procedure has to be iterated from step 2 (see Fig. 10).

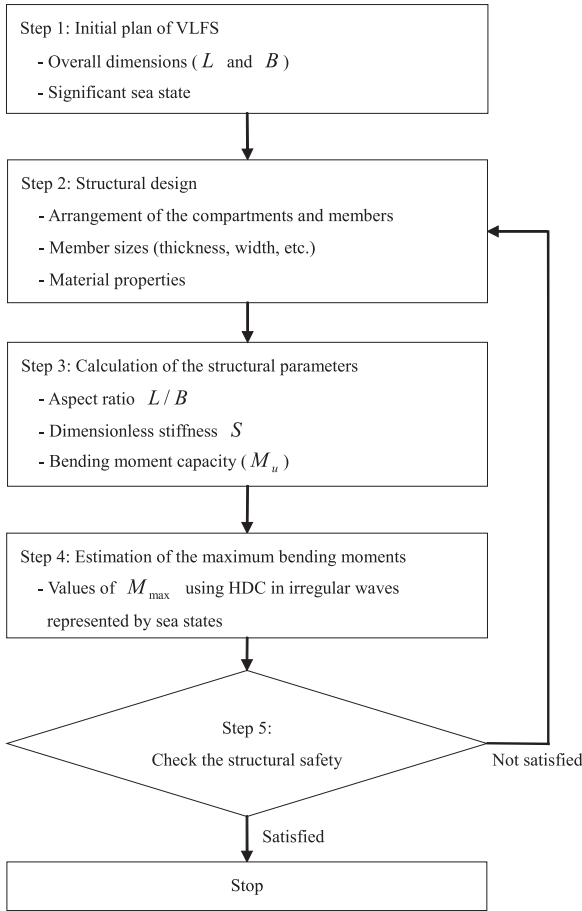


Fig. 10. Preliminary design procedure of VLFSs using HDC.

The proposed design procedure is based on the typical design flows in Fujikubo (2005) and Wang et al. (2008), which require high computational cost for hydroelastic analyses. Mooring effect is not considered in the preliminary design stage. The detailed structural response of the VLFSs to evaluate safety against fatigue and corrosion is considered in the detailed design stage, see Fujikubo (2005) and Wang et al. (2008).

## 5. Design demonstration

HDC just gives the maximum bending moment considering the hydroelastic behavior of VLFSs. Thus, various design methodologies such as ASD (Allowable Stress Design) and LRFD (Load and Resistance Factor Design) can be used to assess the structural safety requirement.

In this section, we demonstrate the preliminary design procedure for the hull girder cross-sections of pontoon-type rectangular VLFSs. In order to check the structural safety, we adopt the rules of LRFD with several assumptions. The hull girder ultimate bending capacity per unit width  $M_u$  has to satisfy

$$\gamma_W(1.86M_{\max}) \leq M_u/\gamma_R \quad (24)$$

in which  $\gamma_W$  and  $\gamma_R$  are the partial safety factors for the design load combinations. Although the partial safety factors have not been well studied for VLFSs, we use  $\gamma_W=1.3$  and  $\gamma_R=1.1$  by the Det Norske Veritas (DNV) rules for ship designs (DNV, 2008). In Eq. (24), the factor 1.86 is also used to calculate the extreme bending moment.

The maximum bending moment  $M_{\max}$  due to the wave conditions can be estimated using HDC considering the significant sea

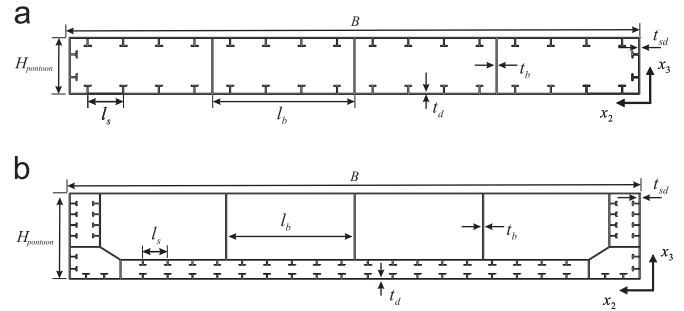


Fig. 11. Hull girder cross-sections along the breadths of the pontoon-type rectangular VLFSs, (a) single hull type and (b) double hull type.

state. The hull girder ultimate bending moment capacity  $M_u$  can be simply calculated by

$$M_u = Z \sigma_{yd} \quad (25)$$

where  $Z$  is the cross-section modulus and  $\sigma_{yd}$  is the minimum yield stress.

### 5.1. Design example: single hull

Let us perform a single hull girder cross-section design of a pontoon type VLFS model of  $L/B=5$ . Length  $L$  is 500 m, breadth  $B$  is 100 m and pontoon height  $H_{\text{pontoon}}$  is 8 m. We assume that the weight of cargos and superstructures  $4100 \text{ kg/m}^2$  is uniformly distributed on the VLFS.<sup>2</sup> We also assume that sea state 6 is the significant condition.

Fig. 11(a) shows the cross-section along the breadth of the VLFS, which has four uniform compartments, that is, the bulkheads are arranged with 25 m intervals in the breadth direction. For the first design trial, the thicknesses of the top and bottom decks, side decks and bulkheads are assumed as  $t_d=13 \text{ mm}$ ,  $t_{sd}=12 \text{ mm}$  and  $t_b=12 \text{ mm}$ , respectively. The T-shape stiffeners are positioned with 2 m intervals in the breadth and height directions, in which the web and flange of the T-shaped stiffener have dimensions of  $600 \text{ mm} \times 15 \text{ mm}$  and  $400 \text{ mm} \times 20 \text{ mm}$ , respectively. Also, the elastic modulus  $E$  is 200 GPa, and Poisson's ratio  $\nu$  is 0.3. The minimum yield stress  $\sigma_{yd}$  is 235 MPa. The steel density is  $8000 \text{ kg/m}^3$ . For the simplicity of the design demonstration, we only change the thickness of top and bottom decks  $t_d$  in the iteration of design procedures.

From the cross-section design of the first trial, the second moment of inertia  $I$  and the dimensionless bending stiffness  $S$  are calculated to be  $63.1 \text{ m}^4$  and  $4 \times 10^{-5}$ , respectively. The bending moment capacity  $M_u$  is also calculated using Eq. (25), see Table 3. We now can estimate the dimensionless maximum bending moments  $\bar{M}_{\max}^{(6)}$  using HDC as shown in Fig. 7(b). Note that HDC gives the dimensionless values. Thus, the physical values  $M_{\max}$  should be calculated using Eqs. (15) and (22)

$$M_{\max} = \rho_w g L^2 a_{1/3} \bar{M}_{\max}^{(6)} \quad (26)$$

In the first trial, the safety factor  $SF = (M_u/\gamma_R)/(\gamma_W \times 1.86M_{\max})$  is calculated as 0.76, which means that the safety condition in Eq. (24) is not satisfied. Thus, the thickness of the top and bottom decks  $t_d$  should be adjusted, and the second and third trials are listed in Table 3. Iterating the design procedures, the hull girder cross-section of VLFS designed in the third trial ( $t_d=33.5 \text{ mm}$ ) not only satisfies the safety requirement but also gives the most reasonable safety factor 1.16 among the three trials.

<sup>2</sup> Note that the self-weight is also reflected in dead load with the weight of cargos and superstructures.

The cross-section design along the length can be considered as a simple extension of the cross-section design along the breadth. Thus, the cross-section along the length has 20 uniform compartments with the same dimensions of bulkheads and desks as the cross-section along the breadth has.

To check the predictive capability of the HRC-II and HDC proposed in this paper,  $\bar{M}_{\max}$  and  $\bar{M}_{\max}^{(6)}$  estimated by HRC-II and HDC are compared with the bending moments calculated through 10,200 cases of hydroelastic analysis for the third trial model ( $S=8.1 \times 10^{-5}$ ). In the numerical analysis, the floating plate model is discretized by a  $60 \times 12$  uniform mesh. The ratio of draft to structural depth  $d/H$  is 0.5875 with self-weight in the third trial model.

Length  $L$ , the second moment of inertia  $I$ , and elastic modulus  $E$  of the plate model are identical to those of the pontoon-type VLFS, but height  $H$ , draft  $d$  and, structural density  $\rho_s$  of the plate model are equivalently calculated by

$$H = \left( \frac{12I_{\text{pontoon}}}{B} \right)^{1/3}, \quad d = \frac{d_{\text{pontoon}}}{H_{\text{pontoon}}}, \quad \rho_s = \frac{d}{H} \rho_w, \quad (27)$$

The same ranges of dimensionless wave length and angle ( $0.04 \leq \alpha \leq 2$  and  $0 \sim 90^\circ$ ) are considered.

It is very important to note that the HRC-II and HDC were developed under the assumptions of infinite water depth and draft  $d/H=0.5$ . These assumptions can cause the differences between estimated and calculated maximum bending moments. Of course, human eye reading error is also involved in the differences. Based on the third design trial, we consider 4 cases as listed in Table 4: (I), (II), (III) and (IV). In the cases (I) and (II), the draft  $d/H=0.5875$  is considered. The calculated maximum bending moments are 3.6–5.9% larger than the estimated maximum bending moments. The differences are not so large for the preliminary design purpose.

**Table 3**  
Design trials of the pontoon-type rectangular VLFS with single hull cross-section, see Figs. 7(b) and 11(a).

	Trial #1	Trial #2	Trial #3
Step 3			
$t_d$ (mm)	13	53.5	33.5
$S$	$4.0 \times 10^{-5}$	$12.0 \times 10^{-5}$	$8.1 \times 10^{-5}$
$d/H$	0.5475	0.6263	0.5875
$M_u$ (MNm/m)	37.1	110.8	73.8
Step 4			
$\bar{M}_{\max}^{(6)}$	$5.8 \times 10^{-3}$	$8.6 \times 10^{-3}$	$7.6 \times 10^{-3}$
Step 5			
$\gamma_w(1.86M_{\max})$ (MNm/m)	44.1	65.3	57.7
$M_{ul}/\gamma_R$ (MNm/m)	33.7	100.7	67.1
Safety factor (SF)	0.76	1.54	1.16

**Table 4**  
Comparison between the dimensionless maximum bending moments estimated by HRC-II and HDC and those calculated by hydroelastic analyses, see Figs. 6 and 7(b).

	Estimated	Calculated			
		(I)	(II)	(III)	(IV)
$h$	Inf.	Inf.	50 m	50 m	10 m
Water depth range	–	–	Intermediate to deep	Intermediate to deep	Shallow to intermediate
Draft ( $d/H$ )	0.5	0.5875	0.5875	0.5	0.5
$\bar{M}_{\max}$	$9.9 \times 10^{-3}$	$10.52 \times 10^{-3}$	$10.47 \times 10^{-3}$	$10.41 \times 10^{-3}$	$12.79 \times 10^{-3}$
		Diff.= 5.9%	Diff.= 5.4%	Diff.= 4.9%	Diff.= 22.6%
$\bar{M}_{\max}^{(6)}$	$7.6 \times 10^{-3}$	$7.89 \times 10^{-3}$	$7.88 \times 10^{-3}$	$7.83 \times 10^{-3}$	$9.30 \times 10^{-3}$
		Diff.= 3.7%	Diff.= 3.6%	Diff.= 2.9%	Diff.= 18.3%
Difference = $\frac{ \text{Calculated} - \text{Estimated} }{ \text{Calculated} } \times 100\%$					

Considering two finite water depth cases: (III)  $h=50$  m and (IV)  $h=10$  m, we test the feasibility of the proposed HRC-II and HDC. Based on the ratio of water depth to wave length ( $h/\lambda$ ), the water depth can be categorized into shallow, intermediate and deep water ranges. The water depth  $h$  is represented by a dimensionless variable  $\beta=h/L$ . Then,  $h/\lambda$  becomes the ratio of  $\beta$  to  $\alpha$  ( $=\lambda/L$ ), that is,  $h/\lambda=\beta/\alpha$ . Fig. 12 shows the three water depth ranges. For the range of dimensionless wave length ( $0.04 \leq \alpha \leq 2$ ) considered in the HRCs and HDC, the water depth ranges for  $h=50$  m and 10 m are given in Fig. 12(a) and (b), respectively. The ranges for  $h=50$  m and  $h=10$  m are included in the intermediate and deep water ranges and in the shallow and intermediate water ranges, respectively. We here note that the water depth ranges of three previous VLFS designs in Table 1 are mostly included in the intermediate water range, see Fig. 12(c), (d) and (e).

Table 4 shows the dimensionless maximum bending moments  $\bar{M}_{\max}$  and  $\bar{M}_{\max}^{(6)}$  estimated by HRC-II and HDC, see Figs. 6 and 7(b). The differences between calculated and estimated values are 2.9–4.9% and 18.3–22.6% for  $h=50$  m and 10 m, respectively. These results show that HRC-II and HDC could provide reasonable preliminary designs of VLFSs when water depth ranges are not largely included in the shallow water range.

### 5.2. Design example: double hull

We here demonstrate one more preliminary design case for a pontoon type VLFS model with a double hull cross-section. LRFD is also applied in this design example. Length  $L$  is 600 m, breadth  $B$  is 80 m ( $L/B=7.5$ ) and pontoon height  $H_{\text{pontoon}}$  is 10 m. We assume that the ratio of draft to structural depth  $d/H$  is fixed as 0.5, and then sea state 5 is considered as the significant condition.

Fig. 11(b) shows the cross-section along the breadth of the VLFS, which has four uniform compartments ( $l_b=20$  m). For the first trial, the thicknesses of the top and bottom decks, side decks and bulkheads are assumed to be  $t_d=14$  mm,  $t_{sd}=14$  mm and  $t_b=10$  mm, respectively. The T-shape stiffeners are positioned with 1.7 m intervals in the breadth and height directions, in which the web and flange of the T-shaped stiffener have dimensions of 250 mm  $\times$  12 mm and 90 mm  $\times$  16 mm, respectively. Material properties are the same as in the single hull case. For the simplicity of the design demonstration, we here change the thicknesses of decks ( $t_d$ ,  $t_{sd}$  and  $t_b$ ) in the iteration of design procedures.

The three design trials are summarized in Table 5. In the first trial, the safety factor  $SF$  is calculated as 1.01, in which the safety margin is too small. Thus, we perform additional design trials. In the third trial, we obtain the double hull girder cross-section with  $SF=1.27$ .

Finally, we give remarks on the use of the principal bending moments in the HRCs and HDC. Since the proposed HRCs and HDC are based on the maximum principal bending moments, the direction of the cross-section in which the maximum principal

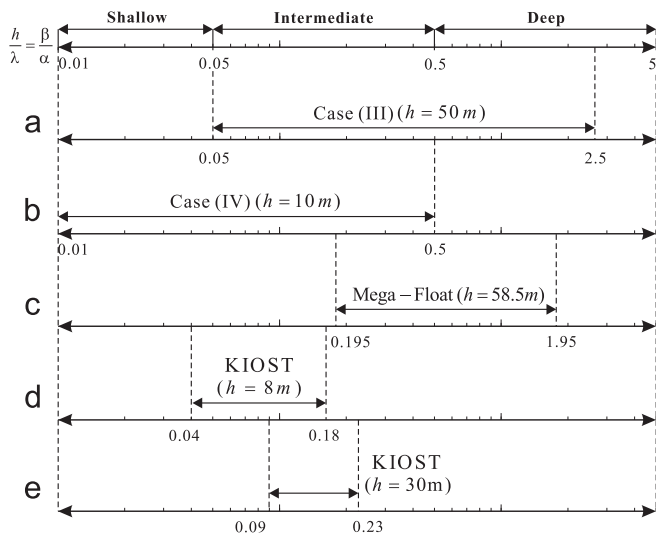


**Fig. 12.** Water depth ranges. (a) Case (III)  $h=50$  m ( $0.05 \leq \beta/\alpha \leq 2.5$ ), (b) Case (IV)  $h=10$  m ( $0.01 \leq \beta/\alpha \leq 0.5$ ), (c) Mega-Float  $h=58.5$  m ( $0.195 \leq \beta/\alpha \leq 1.95$ ), (d) KIOST  $h=8$  m ( $0.04 \leq \beta/\alpha \leq 0.18$ ), (e) KIOST  $h=30$  m ( $0.09 \leq \beta/\alpha \leq 0.23$ ).

**Table 5**

Design trials of the pontoon-type rectangular VLFS with double hull cross-section, see Figs. 7(a) and 11(b).

	Trial #1	Trial #2	Trial #3
<b>Step 3</b>			
$t_d$ (mm)	14	36	21
$t_{sd}$ (mm)	14	36	21
$t_b$ (mm)	10	33	15
$S$	$2.0 \times 10^{-5}$	$5.0 \times 10^{-5}$	$3.0 \times 10^{-5}$
$d/H$	0.5	0.5	0.5
$M_u$ (MNm/m)	45.94	114.84	68.90
<b>Step 4</b>			
$\bar{M}_{\max}^{(6)}$	$5.7 \times 10^{-3}$	$8.2 \times 10^{-3}$	$6.8 \times 10^{-3}$
<b>Step 5</b>			
$\gamma_w (1.86M_{\max})$ (MNm/m)	41.16	59.21	49.10
$M_u/\gamma_R$ (MNm/m)	41.76	104.40	62.64
Safety factor (SF)	1.01	1.76	1.27

bending moment occurs does not coincide with that of the design cross-section considered. This means that the use of HDC would result in a slightly conservative structural design, especially when  $L/B$  is not large (close to 1.0).

## 6. Concluding remarks

In this study, we developed design tools that can significantly reduce the computational cost for hydroelastic analyses of VLFSs at the preliminary design stage. For this purpose, we extensively performed well-established hydroelastic analyses of rectangular floating plates. Water depth was assumed to be infinite, and the draft was fixed as half of the structural depth.

We first constructed two types of hydroelastic response contours (HRC-I and HRC-II), which, for the given structural parameters, can estimate the RAO of the dimensionless maximum bending moment in regular waves. Based on the HRCs, the hydroelastic design contour (HDC) was developed to predict the maximum principle bending moment of VLFSs in irregular waves represented by sea states. Here, we assume the practical ranges of the wave parameters.

The maximum bending moments predicted through HDC can be used for the preliminary design of VLFSs. We also proposed a preliminary design procedure using HDC instead of time-consuming numerical analyses to solve the hydroelastic problems of VLFSs. The feasibility of HRCs and HDC was tested through several numerical experiments. The HDC can result in a feasible preliminary cross-section design and significantly reduce engineers' effort and time at the preliminary design stage of VLFSs.

To construct the HDC in this study, we made the several assumptions regarding ocean environments, structural parameters, and wave parameters. It is important to note that the feasibility of HDC would depend on the differences between actual and assumed conditions. Of course, additional studies on the differences are required as a future study, and an excellent research topic would be the construction of HDC for large ships by applying a procedure similar to that presented in this paper.

## Acknowledgment

This research was supported by a grant [NEMA-ETH-2012-05] from the Earthquake and Tsunami Hazard Mitigation Research Group, National Emergency Management Agency of Korea. This research was also supported by the Basic Science Research Program through the National Research Foundation of Korea (NRF) funded by the Ministry of Science, ICT and Future Planning (No. 2011-0014387).

## References

- Bathe, K.J., Dvorkin, E.N., 1986. A formulation of general shell elements—the use of mixed interpolation of tensorial components. *Int. J. Numer. Methods Eng.* 22, 697–722.
- Bathe, K.J., 1996. *Finite Element Procedures*. Prentice Hall, New York.
- Bathe, K.J., Lee, P.S., 2001. Measuring the convergence behavior of shell analysis schemes. *Comput. Struct.* 89, 285–301.
- Bathe, K.J., Lee, P.S., Hiller, J.F., 2003. Towards improving the MITC9 shell element. *Comput. Struct.* 81, 477–489.
- Bishop, R.E.D., Price, W.G., 1979. *Hydroelasticity of Ships*. Cambridge University Press, Cambridge.
- Dean, R.G., Dalrymple, R.A., 1984. *Water Wave Mechanics for Engineers and Scientist*. Prentice Hall, New Jersey.
- DNV, 2008. Rules for Classification of Ships. IACA common structural rules.
- Fujikubo, M., 2005. Structural analysis for the design of VLFS. *Mar. Struct.* 18, 201–226.
- Hong, S.Y., 2007. Design Manual for Very Large Floating Structures. KIOST, Daejeon.
- ISSC, 2006. Report of Special Committee VL2 “Very Large Floating Structures”. In: *Proceeding of the 16th International Ship and Offshore Structure Congress*. Southampton, United Kingdom.
- Journée, J.M.J., Massie, W.W., 2001. *Offshore Hydrodynamics*. Delft University of Technology, Delft.
- Kashiwagi, M., 1998. A B-spline Galerkin scheme for calculating the hydroelastic response of a very large floating structure in waves. *J. Mar. Sci. Technol.* 3, 37–49.
- Khabakhpasheva, T.I., Korobkin, A.A., 2002. Hydroelastic behaviour of compound floating plate in waves. *J. Eng. Math.* 44, 21–40.
- Kim, B.W., Hong, S.Y., Kyoung, J.H., Cho, S.K., 2007. Evaluation of bending moments and shear forces at unit connections of very large floating structures using hydroelastic and rigid body analyses. *Ocean. Eng.* 34, 1668–1679.
- Kim, J.G., Zi, G., Lee, P.S., 2011. Development of design charts for very large floating structures. In: *Proceeding 21th International Offshore and Polar Engineering Conference*. Hawaii, USA.
- Kim, K.T., Lee, P.S., Park, K.C., A direct coupling method for 3D hydroelastic analysis of floating structures. *Int. J. Numer. Methods Eng.* 96, 2013, 842–866.
- Lee, C.H., Newman, J.N., 2000. An assessment of hydroelasticity for very large hinged vessels. *J. Fluid Struct.* 14, 957–970.
- Lee, P.S., Bathe, K.J., 2004. Development of MITC isotropic triangular shell finite elements. *Comput. Struct.* 82, 945–962.
- Lee, P.S., Noh, H.C., Bathe, K.J., 2007. Insight into 3-node triangular shell finite elements: the effects of element isotropy and mesh patterns. *Comput. Struct.* 85, 404–418.
- Lee, P.S., Bathe, K.J., 2010. The quadratic MITC plate and MITC shell elements in plate bending. *Adv. Eng. Softw.* 41, 712–728.
- Lee, Y.G., Yoon, K.H., Lee, P.S., 2012. Improving the MITC3 shell finite element by using the Hellinger–Reissner principle. *Comput. Struct.* 110, 93–106.
- Riggs, H.R., Niimi, K.M., Huang, L.L., 2007. Two benchmark problems for three-dimensional, linear Hydroelasticity. *J. Offshore Mech. Arct. Eng.* 129, 149–157.

- Taylor R., Eatock, 2007. Hydroelastic analysis of plates and some approximations. *J. Eng. Math.* 58, 267–278.
- Timoshenko, S.P., Krieger, W., 1970. *Theory of Plates and Shells*. McGraw-Hill, New York.
- Wang, C.M., Watanabe, E., Utsunomiya, T., 2008. *Very Large Floating Structures*. Taylor & Francis, London and New York.
- Watanabe, E., Utsunomiya, T., Wang, C.M., 2004. Hydroelastic analysis of pontoon-type VLS: a literature survey. *Eng. Struct.* 26, 245–256.
- Wehausen, J.V., Laitone, E.V., 1960. Surface waves. *Encycl. Phys.* 9, 446–778.
- Yago, K., Endo, H., 1996. On the hydroelastic response of box-shaped floating structure with shallow draft. *J. Soc. Naval. Arch. Jpn.* 180, 341–352.